


# Transplantation of sh-miR-199a-5p-Modified Olfactory Ensheathing Cells Promotes the Functional Recovery in Rats with Contusive Spinal Cord Injury

Cell Transplantation  
Volume 29: 1–19  
© The Author(s) 2020  
Article reuse guidelines:  
sagepub.com/journals-permissions  
DOI: 10.1177/0963689720916173  
journals.sagepub.com/home/ccl  


Zhengchao Gao<sup>1</sup> , Yingjie Zhao<sup>1</sup> , Xijing He<sup>1</sup>, Zikuan Leng<sup>2</sup>,  
Xiaoqian Zhou<sup>3</sup>, Hui Song<sup>1</sup>, Rui Wang<sup>1</sup>, Zhongyang Gao<sup>1</sup>,  
Yiqun Wang<sup>1</sup>, Jiantao Liu<sup>4</sup>, Binbin Niu<sup>5</sup>, Haopeng Li<sup>1</sup>,  
Pengrong Ouyang<sup>1</sup>, and Su'e Chang<sup>1</sup>

## Abstract

MicroRNAs (miRNAs) function as gene expression switches, and participate in diverse pathophysiological processes of spinal cord injury (SCI). Olfactory ensheathing cells (OECs) can alleviate pathological injury and facilitate functional recovery after SCI. However, the mechanisms by which OECs restore function are not well understood. This study aims to determine whether silencing miR-199a-5p would enhance the beneficial effects of the OECs. In this study, we measured miR-199a-5p levels in rat spinal cords with and without injury, with and without OEC transplants. Then, we transfected OECs with the sh-miR-199a-5p lentiviral vector to reduce miR-199a-5p expression and determined the effects of these OECs in SCI rats by Basso–Beattie–Bresnahan (BBB) locomotor scores, diffusion tensor imaging (DTI), and histological methods. We used western blotting to measure protein levels of Slit1, Robo2, and srGAP2. Finally, we used the dual-luciferase reporter assay to assess the relationship between miR-199-5p and Slit1, Robo2, and srGAP2 expression. We found that SCI significantly increased miR-199a-5p levels ( $P < 0.05$ ), and OEC transplants significantly reduced miR-199a-5p expression ( $P < 0.05$ ). Knockdown of miR-199a-5p in OECs had a better therapeutic effect on SCI rats, indicated by higher BBB scores and fractional anisotropy values on DTI, as well as histological findings. Reducing miR-199a-5p levels in transplanted OECs markedly increased spinal cord protein levels of Slit1, Robo2, and srGAP2. Our results demonstrated that transplantation of sh-miR-199a-5p-modified OECs promoted functional recovery in SCI rats, suggesting that miR-199a-5p knockdown was more beneficial to the therapeutic effects of OEC transplants. These findings provided new insights into miRNAs-mediated therapeutic mechanisms of OECs, which helps us to develop therapeutic strategies based on miRNAs and optimize cell therapy for SCI.

## Keywords

miRNAs, spinal cord injury, olfactory ensheathing cells, nerve regeneration

<sup>1</sup> Department of Orthopaedics, Second Affiliated Hospital of Xi'an Jiaotong University, Xi'an, Shaanxi Province, China

<sup>2</sup> Department of Orthopaedics, First Affiliated Hospital of Zhengzhou University, Zhengzhou, Henan Province, China

<sup>3</sup> Department of Radiology, Second Affiliated Hospital of Xi'an Jiaotong University, Xi'an, Shaanxi Province, China

<sup>4</sup> Department of Spine and Spinal Cord Surgery, Henan Provincial People's Hospital, Zhengzhou, China

<sup>5</sup> Department of Orthopaedics, Second Affiliated Hospital of Xi'an Medical College, Xi'an, Shaanxi Province, China

Submitted: December 21, 2019. Revised: February 13, 2020. Accepted: February 26, 2020.

## Corresponding Authors:

Su'e Chang and Xijing He, Department of Orthopaedics, Second Affiliated Hospital of Xi'an Jiaotong University, Xi'an, Shaanxi Province 710004, China.  
Emails: suechang@xjtu.edu.cn; xijing\_h@vip.tom.com



Creative Commons Non Commercial CC BY-NC: This article is distributed under the terms of the Creative Commons Attribution-NonCommercial 4.0 License (<https://creativecommons.org/licenses/by-nc/4.0/>) which permits non-commercial use, reproduction and distribution of the work without further permission provided the original work is attributed as specified on the SAGE and Open Access pages (<https://us.sagepub.com/en-us/nam/open-access-at-sage>).

## Introduction

The annual incidence of spinal cord injury (SCI) is 12.1 to 195.4 cases per million around the world<sup>1</sup>. Close to half of the cases are “complete” injuries with little or no motor, sensory, or autonomic function below the injury level. The injury occurs in two stages, a primary insult from trauma, ischemia, or toxins and a secondary injury characterized by inflammatory cascade, accumulation of toxic neurotransmitters, and production of nerve regeneration inhibitory factors. The tissue damage interrupts of ascending and descending nerve fibers, demyelinates propriospinal and other long tracts, followed by gliosis and scarring with impaired function below the injury site<sup>2,3</sup>. SCI prevention, regenerative therapies, and rehabilitation offer limited solutions in today’s medical practice.

The cellular and biochemical mechanisms responsible for SCI largely depend on the activation and inactivation of specific gene programs. MicroRNAs (miRNAs) control gene expression in key processes of SCI<sup>4</sup>, and therapeutic strategies based on miRNAs have attracted increasing interest. In general, miRNAs are small, non-protein-coding RNAs that are 21 to 25 nucleotides in length and can repress translation or induce mRNA degradation of target mRNAs at the post-transcriptional level by binding to the 3’ UTR (untranslated region) of the gene. Aberrantly expressed miRNAs after SCI participate in diverse biological pathways and processes, including cell apoptosis, inflammation, angiogenesis, astrogliosis, oligodendrocyte development, axonal regeneration and remyelination, and oxidative stress responses<sup>5–8</sup>. For example, miR-21 and miR-19b have been reported to be involved in apoptosis and differentiation of neurons<sup>9</sup>; miR-20a, miR-29b, and miR-21 participate in antioxidation and neuroprotection<sup>10,11</sup>; miR-146a, miR-181, and miR-126 play a role in the inflammatory response<sup>12–14</sup>, and miR-21, miR-199a-3p, and miR-9 contribute to axon regeneration and remyelination<sup>15,16</sup>.

Olfactory ensheathing cells (OECs) are born in nasal mucosa, migrate in the olfactory nerve, and usher growing olfactory axons to their destinations in the olfactory bulb. Many investigators<sup>17–19</sup> have reported that OECs also alleviate secondary injury and facilitate functional recovery through multiple mechanisms, including phagocytosis of axonal debris, immunoprotective activity that helps axonal recovery, interactions with glial scar, secretion of neurotrophic factors, stimulation of angiogenesis, extracellular matrix modification, and axon outgrowth and remyelination. Whole-genome transcriptional profiling and large-scale proteomics analyses have provided novel insights how OECs stimulate axon regeneration. Gene expression profile analyses of OECs show activation of many genes that potentially support neurite outgrowth<sup>20</sup>. A proteomics study revealed proteins in OECs-conditioned medium and plasma membrane of OECs may enhance or guide axon regeneration<sup>21</sup>. Proteins that have been found to function in axonal regeneration or guidance include neurotrophic factors, such as

nerve growth factor, brain-derived neurotrophic factor, NT4/5, ciliary neurotrophic factor (CNTF), and GDNF<sup>22–24</sup>; growth factor receptors, including CNTF receptor  $\alpha$ , GFR alpha-1, and GFR alpha-2<sup>22,25</sup>; and axon growth-promoting cell adhesion and extracellular matrix molecules, including CDH2, NCAM1, and LICAM<sup>26,27</sup>, as well as axon guidance molecules, such as netrins, semaphorins, and ephrins<sup>28</sup>.

To date, few studies have focused on the gene expression changes triggered by OEC transplantation in injured spinal cord segments. Torres-Espin et al.<sup>29</sup> analyzed transcriptome changes in the spinal cord by microarray 7 d after a contusion injury and OECs transplantation. By clustering and functional enrichment analyses of mRNAs, they described a regulatory effect of OEC transplantation on tissue repair processes. However, the authors focused on the changes in mRNAs expression rather than miRNAs. The miRNA-mediated therapeutic effects of OECs in SCI rats are not well understood. Based on Torres et al.’s gene expression data (GSE46988)<sup>29</sup>, we analyzed the differential expression of miRNAs in spinal cords with non-SCI, SCI, and OEC transplants. The analysis showed that OEC transplantation partially reversed aberrant expression of miRNAs caused by SCI. For example, miR-199a is upregulated after SCI but downregulated after OEC transplantation while miR-29c is downregulated after SCI but upregulated after OEC transplantation. We, therefore, speculated that downregulation of miR-199a-5p may mediate the therapeutic effects of OECs on SCI rats.

In the present study, we first measured expression levels of miR-199a-5p in vivo and then produced miR-199a-5p-knockdown OECs by transfecting OECs with an sh-miR-199a-5p lentiviral vector. We then assessed the effects of miR-199a-5p-knockdown OECs transplanted into rat spinal cords using BBB scores, imageological and histological examinations, and explored the possible molecular mechanism.

## Materials and Methods

### Animals

The specific-pathogen-free neonatal Sprague-Dawley (SD) rats within 7 d and adult healthy female SD rats were provided by the Experimental Animal Center of Xi’an Jiaotong University of China (Production license No. SCXK [Shaan] 2007-001), and a total of 48 neonatal rats and 69 adult rats were used in this study. This research was approved by the Animal Experiment Committee of Xi’an Jiaotong University (No. 2018-2053). The experimental design is shown in Fig. 1.

### Primary Cultures of OECs and Immunofluorescence

We isolated OECs from olfactory bulb of  $\leq 7$ -d-old SD rat pups, and purified them by the differential cell adhesion method. Briefly, olfactory bulbs were aseptically collected, and the meninges and blood vessels were stripped off with

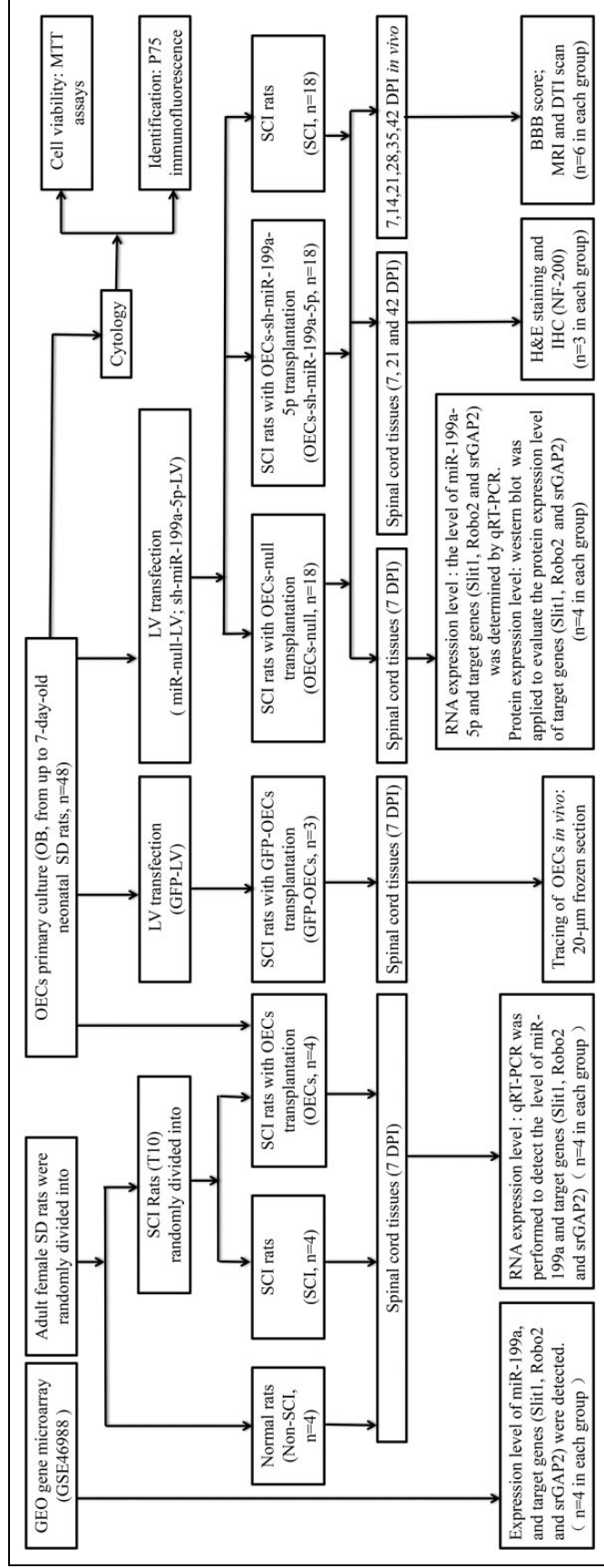


**Fig. 1.** Study design.

DPI: days post injury; DTI: diffusion tensor imaging; GFP: green fluorescence protein; H&E: hematoxylin and eosin; IHC: immunohistochemistry; LV: lentiviral vector; MRI: magnetic resonance imaging; MTT: methyl thiazolyl tetrazolium; OB: olfactory bulb; OECs: olfactory ensheathing cells; qRT-PCR: quantitative real-time polymerase chain reaction; SCI: spinal cord injury; SD: Sprague-Dawley.

fine forceps under a dissection microscope (Nikon, Shanghai, China). Tissues were then dissected into small pieces and centrifuged at 1,200 rpm for 5 min. After that, sediment was enzymatically separated with 0.25% trypsin (Worthington Biochemical, Lake Wood, NJ, USA) for 3 min at 37°C with intermittent agitation. After stopping the digestion, the cells were filtered with a 70- $\mu$ m nylon cell strainer (Jingan Biological Technology Co., Ltd., Shanghai, China) to remove nondissociated tissue pieces and then washed with DF-12 medium (DMEM/F12, Gibco, Gaithersburg, MD, USA) to remove residual enzymes. The cells were recovered by centrifugation, resuspended, and then seeded into uncoated cell-culture dishes (Corning, New York, NY, USA) using medium consisting of 89% DF-12 medium, 10% fetal bovine serum (Gemini Bio-Products, West Sacramento, CA, USA) and 1% penicillin-streptomycin (Sigma-Aldrich, St. Louis, MO, USA). The cells were cultured for 18 h to remove fast-attaching fibroblasts. The supernatant of the first dish was transferred into another uncoated dish for up to 36 h to allow attachment of astrocytes. The final supernatant was seeded onto poly-L-lysine (Sigma-Aldrich)-coated cell-culture dishes to grow primary OECs. Cultures continued until an appropriate cell number was achieved, and the media were changed every 2 d. We used immunofluorescence to determine the purity of OECs. After culture for 5 d, the cells were digested and seeded on 12-mm round, PLL-coated coverslips at a density of 10,000 cells/coverslip. After the cells were grown to 60% to 70% confluency, the cells were washed with preheated phosphate-buffered solution (PBS) followed by incubation of 4% ice-cold paraformaldehyde (Hat Biotechnology, Xi'an, China) for 15 min at room temperature. Nonspecific protein binding was blocked by a 60-min incubation with 10% goat serum albumin (Equitech-Bio Inc., Kerrville, TX, USA), and then cells were incubated overnight at 4°C with primary antibody (rabbit anti-rat p75<sup>NTR</sup> monoclonal antibody, 1:50, Abcam, Cambridge, MA, USA). Cells were washed three times 5 min each time, followed by incubation for 60 min at room temperature with the secondary antibody (goat anti-rabbit DyLight 488 antibody, 1:500, Boster, Wuhan, China). DAPI staining solution (100 ng/ml, Boster) was added for 10 min at room temperature. Coverslips were immediately transferred to glass slides and mounted in mounting medium (Sigma-Aldrich). Thereafter, the coverslips were examined under a fluorescence microscope (Olympus, Tokyo, Japan).

### *Methoxy Thiazolyl Tetrazolium (MTT) Experiment*

After differential adhesion was completed, the OECs were seeded into PLL-coated 96-well plates at a total of 4,000 cells/well in 200  $\mu$ l/well culture medium and were incubated in an incubator containing 5% CO<sub>2</sub> at 37°C, and the medium was replaced every 2 d. A 96-well plate was tested for MTT activity daily. To estimate the quantity of living cells in the cultures, we used the MTT assay. We added 20  $\mu$ l of MTT solution (5 mg/ml, Sigma-Aldrich) to each well of a 96-well

plate, and incubated the cells for 4 h. The supernatant in the duplicate wells was removed, and 150  $\mu$ l of DMSO was added to each well and then with shaking for 10 min. The optical density (OD) value at 570 nm wavelength was then determined on FLUOstar OPTIMA (FLUOstar; BMG Labtech, Offenburg, Germany). The activity of the cells was directly proportional to the absorbance. Each experiment contained six replicates.

### *Lentivirus Transfection*

Primary OECs were seeded into PLL-coated cell-culture dishes at a density of  $2 \times 10^5$ /ml after 5 d of purification. Transfection assays with green fluorescence protein (GFP)-, sh-miR-199a-5p-, and control-lentiviral vectors were conducted to construct GFP-OECs, sh-miR-199a-5p-modified OECs (OECs-sh-miR-199a-5p) and control OECs (OECs-null). The sequence of sh-miR-199a-5p lentiviral vector was 5'-GAACAGGTAGTCTGAACACTGGG-3', and the control lentiviral was an empty vector. All lentiviral vectors were purchased in Hanbio Biotechnology Co., Ltd, Shanghai, China. When the cells were 70% confluent, 20  $\mu$ l of  $2 \times 10^8$  infection function units/ml of GFP-, sh-miR-199a-5p-, and control lentiviral vectors solution were added at a multiplicity of infection of 20 for 24 h. The cells were then cultured in an incubator for 72 h until use. The transfection rate of GFP was observed under a fluorescence microscope and the transfection efficiency of sh-miR-199a-5p was detected by Quantitative real-time polymerase chain reaction (qRT-PCR) 72 h post transfection. The modified OECs were used for transplantation.

### *Animal Model of SCI*

**Animals and Groups.** Adult healthy female SD rats weighing 220 to 250 g were selected for these studies. All rats were allowed preoperative environmental adaptation for 2 wk with normal circadian rhythm and had free access to food and water. For molecular experiments, 12 rats were randomly divided into 3 distinct groups according to the respective intervention: (A) normal rats (non-SCI,  $n = 4$ ), (B) SCI rats (SCI,  $n = 4$ ), and (C) SCI rats with a transplantation of  $5 \times 10^5$  OECs (OECs,  $n = 4$ ). For functional experiments, 54 rats were randomly divided into 3 groups with 18 rats in each group: (A) SCI rats (SCI group,  $n = 18$ ), (B) SCI rats with a transplantation of 9  $\mu$ l of a total of  $5 \times 10^5$  OECs-null (OECs-null group,  $n = 18$ ), (C) SCI rats with a transplantation of the same dose of OECs-sh-miR-199a-5p (OECs-sh-miR-199a-5p group,  $n = 18$ ). An additional three rats received  $5 \times 10^5$  GFP-OECs injections to trace the cells in vivo. Fig. 1 shows the experimental groups.

**Surgical Procedure, Cell Transplantation, and Postoperative Care.** The surgical procedure, spinal cord contusion model, and use of fluids and analgesics followed the steps described in the original publication of the New York University weight-

**Table 1.** Primers and Wild Type or Mutated Target Sequences Used in This Article.

Gene	Forward	Reverse
miR-199a-5p	AGTGTTCACTACCTGTTCA	
U6	GCTTCGGCAGCACATACTAAAAT	CGCTTCACGAATTTGCGTGTTCAT
Slit1	CCGGTGTAGCAACAAGCAC	GTGTGAACTGGTTCCCATCC
Robo2	TACATCTGCCAGGCCCTAAC	GGGTGGAGGTCTATCTGTCAA
SrGAP2	AGTGGGAAGCGGAACCTT	GTCCTTTGCTCCGGTTCAC
Glyceraldehyde 3-phosphate dehydrogenase	GCCAAAAGGGTCATCATCTC	GTAGGCAGGGATGATGTTT
Slit1-3' UTR-WT	CTGCTCATTTCGGGCCTCAGGC	TCGAGCCTGAGGCCCGAAATGAGCAGAGCT
Slit1-3' UTR-MT	CTGCTCATTTCGGGCGAGTCCC	TCGAGGGACTCGCCCGAAATGAGCAGAGCT
Robo2-3' UTR-WT	CATATCAGTGCTCAAAGTCCG	TCGAGCCTGAGTTTGAGCACTGATATGAGCT
Robo2-3' UTR-MT	CATATCAGTGCTCAAAGTCCG	TCGAGGGACTCTTTGAGCACTGATATGAGCT
srGAP2-3' UTR-WT	CGATGAACAGACAGACCACTGGAAC	TCGAGTTCCAGTGGTCTGTCTGTTTCATCGAGCT
srGAP2-3' UTR-MT	CGATGAACAGACAGACCTGACCTTC	TCGAGAAGGTCAGGTCTGTCTGTTTCATCGAGCT

UTR: untranslated region.

drop device<sup>30</sup>. Rats were anesthetized with an intraperitoneal injection of sodium pentobarbital at 40 mg/kg body weight and were subcutaneously administered prophylactic penicillin sodium (20 U/kg) before surgery. The fur was shaved on the middorsal region and cleaned with povidone-iodine solution (Likang Disinfectant Hi-Tech Co., Ltd., Shanghai, China). A 2-cm median incision was made from the mid to low thoracic regions; the muscle and the connective tissue were bluntly dissected to expose the spinous process and lamina from the T8 to L1 vertebra. Laminectomy of the caudal portion of T9 and all of T10 were performed to expose the spinal cord. The cord was then contused with the NYU weight-drop device with an energy of 250 g mm (10 g rod dropped from a height of 25 mm).

For cell transplantation, the OECs, GFP-OECs, OECs – null, and OECs- sh-miR-199a-5p were suspended in DMEM and maintained on ice during the time of surgery. Thirty minutes after the contusion, a total of 9  $\mu$ l suspension containing  $5 \times 10^5$  OECs or modified OECs was intraspinally injected at the epicenter and at 2 mm rostrally and caudally per rat, respectively, using a 10- $\mu$ l Hamilton syringe (Hamilton, Reno, NV, USA) with a glass pipette (100  $\mu$ m inner diameter) held in a micromanipulator. The injection pipette was kept inside the cord tissue for an additional 3 min after each injection to avoid liquid withdrawal. Afterwards, the muscles and skin were sutured in separate layers.

During surgery, body temperature was maintained at 37°C using a controllable heating pad. Immediately after surgery, all rats were subcutaneously given 10 ml normal saline and were monitored until anesthesia recovery. After recovery, two rats were housed per cage, with a 12-h light/dark cycle and free access to food and water. Manual bladder massage was performed twice a day until the micturition reflex recovered, penicillin sodium (20 U/kg) was subcutaneously injected until the hematuria disappeared, and buprenorphine (0.01 mg/kg) was administered daily post surgery by subcutaneous injection for 3 d.

### Tissue Preparation

After in vivo magnetic resonance imaging (MRI) and diffusion tensor imaging (DTI) scans, three rats were randomly selected in each group and were deeply anesthetized with sodium pentobarbital (40 mg/kg intraperitoneally [i.p.]), prior to transcardial perfusion with 4% paraformaldehyde (PFA) at 7, 21, and 42 d post injury (DPI). Approximately 1 cm of spinal cord centered on the injury site was removed and postfixed in PFA for 1 wk. After overnight incubation in 30% sucrose, the tissues were embedded in paraffin, and then 20- $\mu$ m longitudinal tissue sections were sectioned for hematoxylin and eosin (H&E) staining and immunohistochemistry (IHC).

After postfixation in the same fixative solution for 24 h and cryopreservation in 30% sucrose, tissue specimens with transplanted GFP-OECs were longitudinally cryosectioned at 20  $\mu$ m to identify OECs after grafting.

### Total RNA Extraction, Reverse Transcription, and qRT-PCR Analysis

Rats were euthanized at 7 DPI, and 0.5 cm lengths of spinal cord centered on the injury site were rapidly removed and frozen at  $-80^{\circ}\text{C}$  until use. Total RNA was extracted from each group ( $n = 4$ ) of spinal cords or cultured OECs 72 h post transfection using RNAiso Plus (Takara Bio Inc., Otsu, Japan) according to the manufacturer's protocol. cDNA of miRNAs was synthesized from total RNA by using the Mir-X miRNA First-Strand Synthesis Kit (Takara Bio Inc., Otsu, Japan), and cDNA of mRNAs (Slit1, Robo2, and srGAP2) was synthesized using PrimeScript™ RT Master Mix (Takara Bio Inc., Otsu, Japan). qRT-PCR was performed with SYBR® Premix Ex Taq™ II (Takara Bio Inc., Otsu, Japan), and PCR was conducted on a CFX96 Real Time PCR System (Bio-Rad, Hercules, CA, USA). All primers were purchased from Takara. The relative expression of genes was calculated using the  $2^{-\Delta\Delta\text{Ct}}$  method and normalized to U6 or glyceraldehyde 3-phosphate dehydrogenase expression

levels. The primer sequences of genes used in this study are shown in Table 1.

### Total Protein Extraction and Western Blot

Rats were euthanized at 7 DPI, and 0.5 cm lengths of spinal cord centered on the injury site were rapidly removed and frozen at  $-80^{\circ}\text{C}$  until use. Western blot was applied to detect protein expression of Slit1, Robo2, and srGAP2. Total proteins were extracted using a total protein extraction kit (Pioneer Biotechnology, Xi'an, China) according to the manufacturer's recommended protocol. Protein concentration was determined using a bicinchoninic acid protein assay kit (Pioneer Biotechnology). Equal amounts of proteins were separated by sodium dodecyl sulfate-polyacrylamide gels and then transferred to polyvinylidene difluoride membranes (Millipore, Bedford, MA, USA). After blocking in 5% nonfat dry milk in TBST, the membranes were incubated with different primary antibodies at  $4^{\circ}\text{C}$  overnight. The primary antibodies were as follows: anti-Slit1 (1:1000, Bio-Techne, Minneapolis, MN, USA), anti-Robo2 (1:1000, Abcam), anti-srGAP2 (1:100, Abcam), and anti- $\beta$ -actin (1:2000, Zhuangzhi Biotechnology, Xi'an, China). After washing three times with TBST, the membranes were incubated with horseradish peroxidase-conjugated secondary antibodies for 1 h at room temperature. The secondary antibodies were as follows: for Slit1 (1:2000, Zhuangzhi Biotechnology) and for Robo2 and srGAP2 (1:5000, Pioneer Biotechnology), and  $\beta$ -actin (1:5000, Pioneer Biotechnology). The protein bands were developed using a commercially available kit for enhanced chemiluminescence (Aidlab Biotechnology, Beijing, China), and all bands were visualized with a chemiluminescence system (GE Healthcare, Pittsburgh, PA, USA), and data were analyzed using ImageJ (NIH Image, Bethesda, MD, USA). The protein expression levels were normalized to  $\beta$ -actin levels in each sample. All experiments were performed in triplicate to ensure reproducibility.

### Dual-Luciferase Reporter Assay

Potential binding sites for 3'-Slit1-UTR, 3'-Robo2-UTR, 3'-srGAP2-UTR, and miR-199a-5p were predicted by TargetScan ([http://www.targetscan.org/vert\\_71/](http://www.targetscan.org/vert_71/)). The dual-luciferase reporter plasmids pMIRGLO-Slit1 wild-type (Slit1-WT) or pMIRGLO-Slit1 mutant-type (Slit1-MT), pMIRGLO-Robo2 wild-type (Robo2-WT) or pMIRGLO-Robo2 mutant-type (Robo2-MT), pMIRGLO-srGAP2 wild-type (srGAP2-WT) or pMIRGLO-srGAP2 mutant-type (srGAP2-MT) as well as miR-199a-5p mimics and negative control were constructed by RiboBio Co., Ltd. (Guangzhou, China). HEK293 T cells (ATCC, USA) were seeded in a 96-well plate at a density of  $1 \times 10^4$  cells per well 1 d before transfection. For the luciferase assay, the constructed 3'-UTR WT/MT plasmids (400 ng) and miR-199a-5p mimics/negative control (100 nmol/l) were cotransfected into 293 T cells using Lipofectamine 3000

(Invitrogen, Carlsbad, CA, USA) according to the manufacturer's protocol. After 24 h of transfection, firefly and Renilla luciferase activities were measured using the Dual-Glo luciferase assay system (Promega, Shanghai, China) according to the manufacturer's instructions. The relative firefly luciferase activity was normalized by Renilla luciferase activity. The wild-type or mutated target sequences used in this article are shown in Table 1.

### MRI, DTI Scan, and DTI Analysis

**MRI and DTI Scans.** All scans were performed on a 3.0-Tesla MR scanner (Sigma; GE Medical Systems, Milwaukee, WI, USA) using a dedicated animal coil designed for scanning rats. An MRI scan was conducted at 7, 21, and 42 DPI, and a DTI scan was scheduled at 72 h before surgery and weekly post SCI. Six rats randomly selected from 54 healthy rats for DTI scan to obtain DTI parameters of normal rats at 72 h before SCI and 18 rats (6 rats per group) were randomly chosen to perform the MRI and DTI scans post SCI. The animals were anesthetized with sodium pentobarbital (40 mg/kg i.p.) and placed in the coil in a supine position to minimize the influence of respiratory movement on magnetic resonance artifacts of the spinal cord. For conventional MRI, an SE sequence was used to acquire T1-weighted and T2-weighted images (T1WI and T2WI). The parameters for sagittal T1WI were as follows: TR/TE of 440 ms/11.1 ms, image matrix of  $256 \times 256$ , and five contiguous slices with a slice thickness of 1.5 mm. Sagittal T2WI was acquired using the following parameters: TR/TE of 2200 ms/126 ms, image matrix of  $256 \times 256$ , and five contiguous slices with a slice thickness of 1.5 mm. For DTI, a single-shot spin-echo echo-planar imaging sequence was applied to acquire the images, and the scanning parameters were as follows: diffusion-weighted coefficient ( $b$ -value) = 1000  $\text{s}/\text{mm}^2$ ; diffusion-sensitive gradient = 25 different directions; repetition time = 3500 ms; echo time = 87.5 ms; thickness = 2.4 mm; space = 0; field of view = 10; acquisition matrix =  $64 \times 64$ .

**DTI Analysis.** After scanning, the data were transferred to an independent workstation (Advantage Windows Workstation, version 4.2, GE Healthcare, Waukesha, WI, USA) and post-processed by two radiologists who were blinded to the study. The quantitative DTI parameter, fractional anisotropy value (FA value), was obtained on a workstation using the software Functool™ provided by GE Medical Systems by using regions of interest. Diffusion tensor tractography (DTT) of the spinal cord was generated using the FACT algorithm implemented in Volume-One software. The FA threshold was less than 0.2 and the stopping angle was more than  $25^{\circ}$ .

### H&E Staining

Longitudinal sections were deparaffinized and rehydrated in a decreasing series of ethanol washes (5 min each) and then

submerged in hematoxylin for 4 min. The sections were washed in water followed by 1% HCl in ethanol solution for 30 s. Subsequently, the sections were washed with water again and stained with eosin for 6 min. Finally, the sections were dehydrated in 80%, 85%, 90%, and 100% ethanol (5 min each) and mounted with DPX (Sigma-Aldrich).

### Immunohistochemical Staining

Serial longitudinal tissue sections of 20  $\mu\text{m}$  thickness were cut, and we selected three slices from each rat to perform neurofilament-200 (NF200) immunohistochemical staining. Briefly, the sections were deparaffinized, rehydrated in distilled water, placed in 3% hydrogen peroxide to remove endogenous peroxidase activity, and then rinsed with PBS three times for 5 min each time. The slices were blocked with 10% normal goat serum for 15 min following permeabilization with 0.1% Triton X-100. Afterwards, monoclonal mouse anti-NF200 antibody (1:1000; Sigma-Aldrich) was used. The sections were incubated at 4°C overnight in primary antibody. The sections were then washed three times with 0.1 M PBS (pH 7.4) and incubated with a rabbit anti-mouse secondary antibody (1:1000, Beijing Biosynthesis, Beijing, China) for 1 h at room temperature. Specific staining was visualized with diaminobenzidine according to the supplier's instructions (Beyotime, Shanghai, China), followed by counterstaining with hematoxylin. Finally, sections were washed with PBS, dehydrated through a graded alcohol series (50%, 75%, 95%, and 100%), cleared with dimethylbenzene, and mounted using a coverslip.

For analysis, six randomly selected fields were imaged at 200 $\times$  magnification under a microscope (Olympus, Tokyo, Japan). Negative controls were processed according to the same protocol, but the primary antibody was omitted. Images of NF200-stained sections were imported into Image J software (NIH Image, Bethesda, MD, USA) to quantify the positively stained area.

### Behavioral Assessment

Behavioral assessment was evaluated using the open-field Basso–Beattie–Bresnahan Locomotor Rating Scale (BBB score). The hindlimb movements of all rats were tested at least once a week from 1 DPI to 42 DPI and recorded through video by an independent researcher, and the locomotor BBB scores were evaluated by two other well-trained individuals who were blinded to the study. Eighteen rats (six rats per group) were randomly chosen to acquire BBB scores. The average locomotion score of the bilateral hind limbs was calculated as the final score for each rat at each time point.

### Statistical Analysis

Variables were presented as the mean  $\pm$  standard errors of the means from at least three independent experiments with  $n$  representing the number of replicates. A one-way analysis

of variance (ANOVA) or two-way ANOVA was used to evaluate the statistical significance of multiple-group comparisons, and comparisons between two groups were conducted using a Student's–Newman–Keuls test ( $q$  test) if values were normally distributed, or Kruskal–Wallis  $H$  rank sum test if not. The Shapiro–Wilk test was used to determine whether the data followed a normal distribution. All statistical calculations were performed using SPSS 23.0 software (SPSS Inc, Chicago, IL, USA), and all graphs were generated by GraphPad Prism 5.0 (GraphPad Software Inc., San Diego, CA, USA) and Photoshop CS6 (Adobe, San Jose, CA, USA). A  $P$ -value  $<0.05$  was considered statistically significant.

## Results

### Primary Cultures of OECs and Identification In Vitro and In Vivo

We cultured primary OECs from the olfactory bulb of newborn SD rats within 7 d by differential cell adhesion (Fig. 2A–G). Then, we used P75<sup>NTR</sup> immunofluorescence to identify the OECs *in vitro*. Five different regions were randomly selected under fluorescence microscopy to determine the purity of OECs by comparing the number of DAPI-labeled nuclei with P75<sup>NTR</sup> immunoreactive cells, and the results demonstrated that  $94.3\% \pm 3.34\%$  of cells were P75<sup>NTR</sup>-positive OECs (Fig. 2D, F). Cell activity experiments were measured by the MTT method to determine the optimal time for OEC transplantation, and the results indicated the optimal time window for OEC transplantation was from the 8th day to the 10th day after differential cell adhesion, at which time OECs showed good activity and less fibroblast contamination. A representative image of primary OECs on the 9th day after differential cell adhesion is presented in Fig. 2C. As shown in Fig. 2C, OECs exhibited a typical bipolarity or multipolarity under phase-contrast microscopy, with a clear outline. The cell body was translucent, with strong refractive properties, and the neurites were particularly obvious and plentiful and intertwined into a network. Therefore, all cell transplantation experiments in this study were performed on the 9th day after differential cell adhesion. To trace the grafted OECs, we performed an *in vivo* tracing experiment of grafted OECs, which were transfected with a GFP lentiviral vector. GFP<sup>+</sup> OECs after 72 h of transfection are shown in Fig. 2G, and the transfection efficiency was almost 100% under a fluorescence microscope. After GFP<sup>+</sup> OECs were grafted for 7 d, spinal cord segments centered on the injury site were longitudinally cryosectioned at a thickness of 20  $\mu\text{m}$  to determine the localization of OECs under fluorescence microscopy. The localization of GFP<sup>+</sup> OECs is shown in Fig. 2H, indicating that a large number of GFP<sup>+</sup> OECs were localized around the lesion, although the cells in the injury center had died. Moreover, we found that the OECs



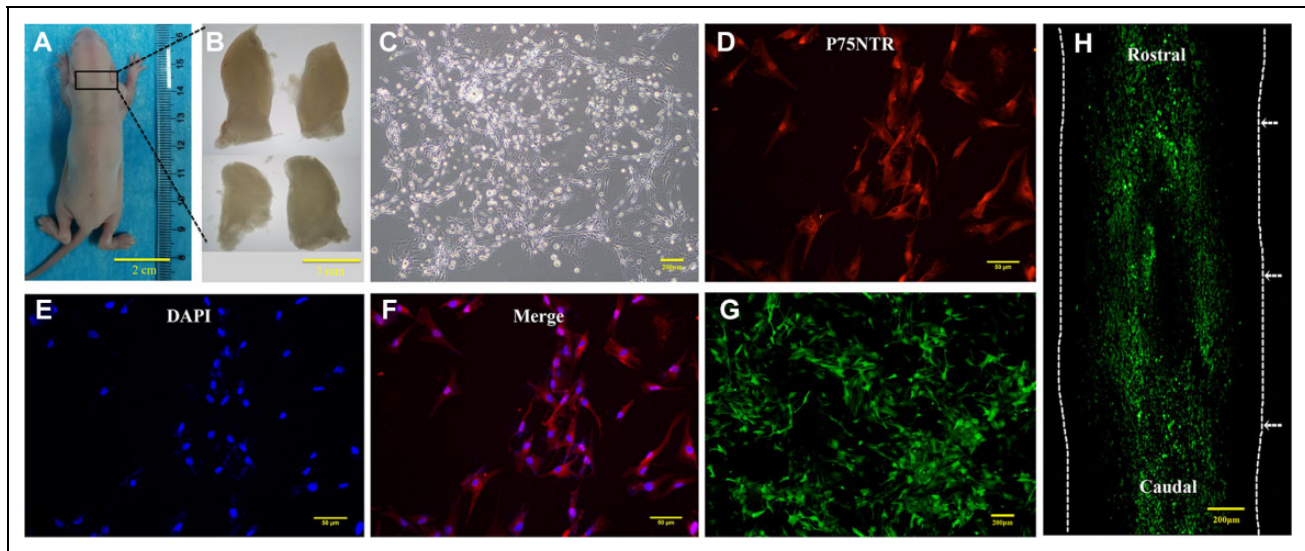


**Fig. 2.** Primary culture and identification of olfactory bulb OECs from newborn SD rats and in vivo tracing of grafted OECs. (A) Newborn SD rats within 7 d. (B) Olfactory bulbs before and after stripping the meninges and blood vessels. The scale bar is 3 mm. (C) Cultured OECs on the 9th day after differential cell adhesion under a phase-contrast microscope. The scale bar is 200  $\mu$ m. (D–F) P75NTR immunoreactive OECs with nuclear staining (DAPI). The scale bar is 50  $\mu$ m. (G) GFP-positive OECs after 72 h of transfection with the GFP lentiviral vector. (H) The surviving OECs in injured spinal cord at 7 d post GFP<sup>+</sup> OEC transplantations. The white dotted line represents the border of the injured spinal cord, and the arrow represents the injection site of OECs. The scale bar is 200  $\mu$ m. GFP: green fluorescence protein; OEC: olfactory ensheathing cell; SD: Sprague-Dawley.

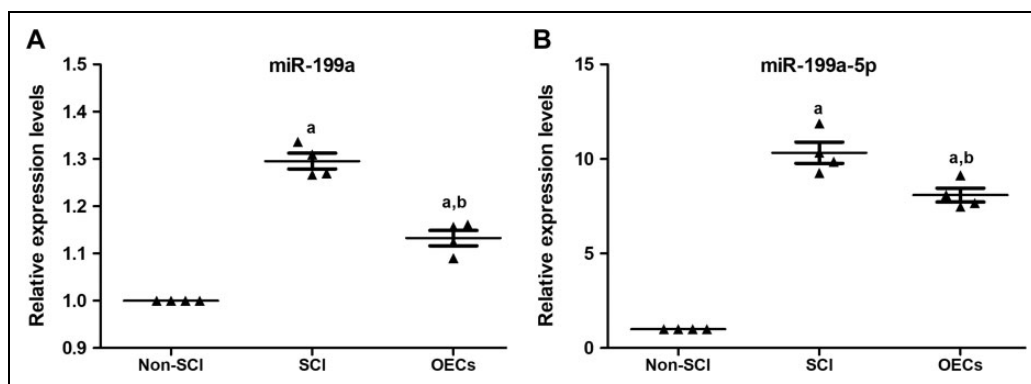


**Fig. 3.** OEC transplantation downregulates the expression of miR-199a-5p. (A) Relative expression levels of miR-199a in the spinal cord with non-SCI, SCI, and OEC transplantation for 1 wk based on microarray data (GSE46988, <https://www.ncbi.nlm.nih.gov/geo>). (B) Relative expression levels of miR-199a-5p in the spinal cord with non-SCI, SCI, and OEC transplantation for 1 wk was determined by quantitative real-time polymerase chain reaction. All results are expressed as the mean  $\pm$  SEM from four independent experiments ( $n = 4$ ). <sup>a</sup> $P < 0.05$  vs non-SCI group; <sup>b</sup> $P < 0.05$  vs SCI group. OEC: olfactory ensheathing cell; SCI: spinal cord injury.

migrated from the injection site along the longitudinal axis of the spinal cord (Fig. 2H).

### OEC Transplantation Downregulates the Expression of miR-199a-5p

We analyzed differential expression of miRNAs in rat spinal cords with and without injury, with and without OEC transplantation in Gene Expression Omnibus (GSE46988).

Microarray analysis revealed that the miR-199a levels in SCI group were significantly higher than that in the non-SCI group ( $P < 0.05$ ). Conversely, miR-199a was significantly downregulated after OEC transplantation compared with that in the SCI group ( $P < 0.05$ ) (Fig. 3A). The findings indicated that OEC transplantation reversed the miR-199a levels. To verify and extend this finding, we measured the miR-199a-5p expression levels at 7 d post OEC transplantation by qRT-PCR. The results showed a high agreement with



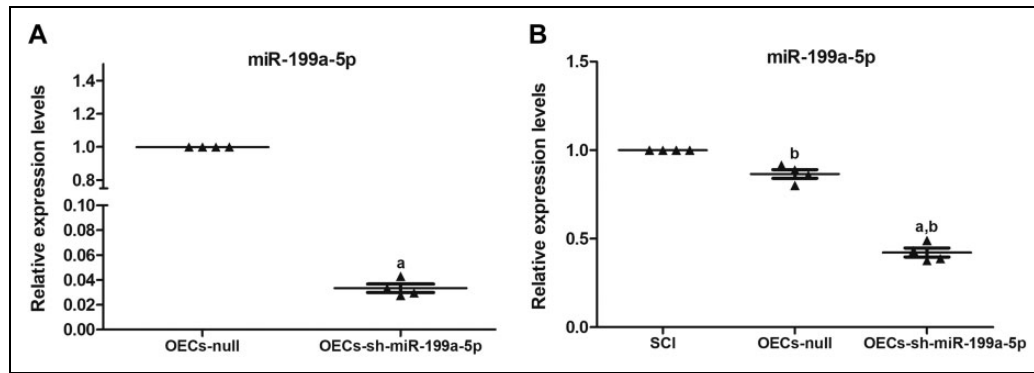


**Fig. 4.** Relative expression of miR-199a-5p in modified OECs and the injured spinal cord. (A) Relative expression of miR-199a-5p in OECs after transfecting with control (OECs-null) or sh-miR-199a-5p lentiviral vector (OECs-sh-miR-199a-5p). (B) Relative expression of miR-199a-5p in spinal cords with SCI, OECs-null, or OECs-sh-miR-199a-5p transplantation. All qRT-PCR data are presented as the mean  $\pm$  standard error of the mean from four independent experiments ( $n = 4$ ). <sup>a</sup> $P < 0.05$  vs OECs-null group, <sup>b</sup> $P < 0.05$  vs SCI group. OEC: olfactory ensheathing cell; SCI: spinal cord injury.

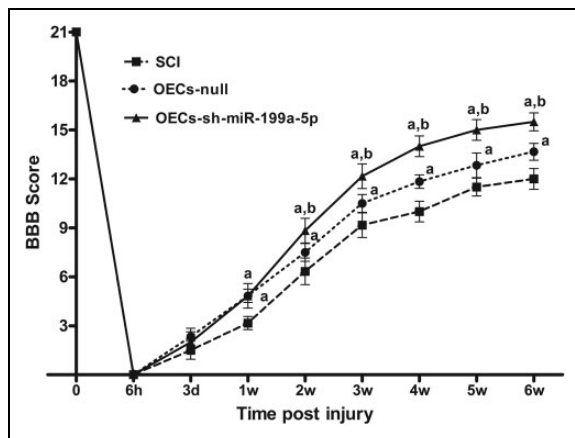


**Fig. 5.** Transplantation of sh-miR-199a-5p-modified OECs improves BBB scores. The number of rats for each group at each point is 6. Data are represented as the mean  $\pm$  standard deviation. <sup>a</sup> $P < 0.05$  vs SCI group; <sup>b</sup> $P < 0.05$  vs OECs-null group. BBB: Basso-Beattie-Bresnahan; OEC: olfactory ensheathing cell; SCI: spinal cord injury.

the microarray results, namely, the relative miR-199a-5p levels in the SCI group were more than 10-fold higher compared to that in the non-SCI group ( $P < 0.05$ ), and significantly lower compared to the SCI group ( $P < 0.05$ ) (Fig. 3B). Therefore, we can conclude that OEC transplantation reduced the miR-199a-5p expression. Based on this finding, we speculated that downregulation of miR-199a-5p may mediate the therapeutic effects of OECs on rats with contusive SCI.

### Knockdown of miR-199a-5p Promotes Functional Recovery in Rats with SCI

After 72 h of OECs transfected with sh-miR-199a-5p- or control-lentiviral vector, we measured gene-knockdown

efficiency in modified OECs by qRT-PCR. The results showed that the gene-knockdown efficiency was 96.54%, and the miR-199a-5p levels in miR-199a-5p knockdown OECs were significantly inhibited compared to that in OECs-null ( $P < 0.05$ ) (Fig. 4A). Thirty minutes after SCI, OECs-null or OECs-sh-miR-199a-5p were transplanted by intraspinal injection. After 7 d, we also measured the miR-199a-5p levels in injured spinal cord of each group. Our data illustrated that the miR-199a-5p levels in OECs-sh-miR-199a-5p-transplanted group were also significantly inhibited compared to that in the OECs-null-transplanted group ( $P < 0.05$ ), and both were significantly lower compared with that in the SCI group ( $P < 0.05$ ) (Fig. 4B). These results indicated that our transfection and transplantation experiments were reliable and credible. We then evaluated the therapeutic effects of the modified OECs for treating SCI.

### Hindlimb Motor Function

Hindlimb motor function was evaluated by the BBB score before SCI and 6 h, 3 d, and weekly until 6 wk after SCI. The BBB score was significantly decreased after contusive SCI and gradually increased with time in all three groups (Fig. 5). The results showed that the BBB scores in the OECs-sh-miR-199a-5p and OECs-null groups were significantly higher than those in the SCI group from 1 wk post transplantation ( $P < 0.05$ ). Moreover, the scores of the OECs-sh-miR-199a-5p group began to increase compared to those of the OECs-null group from 2 wk after transplantation ( $P < 0.05$ ) (Fig. 5), indicating that knockdown of miR-199a-5p in OECs promoted lower-extremity motor function in rats with contusive SCI.

### Conventional MR Images

We used MRI to visualize the effects of the modified OECs for treatment of SCI. The hypointense region in the T1WI

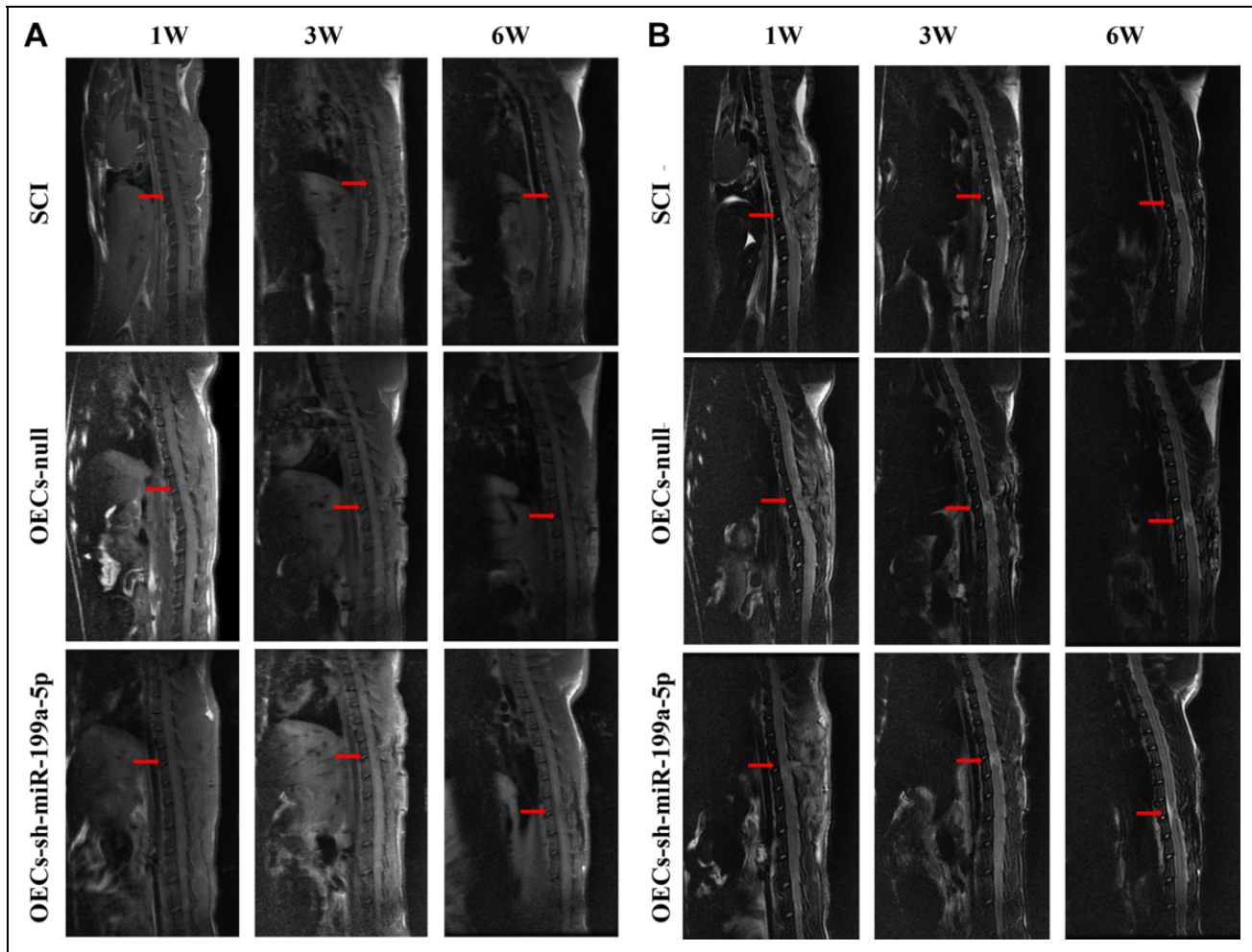


**Fig. 6.** Representative magnetic resonance images of rats in each group. (A) T1-weighted images of the spinal cord after a contusive injury. (B) T2-weighted images of the spinal cord after a contusive injury. Red arrows represent the injured site. OEC: olfactory ensheathing cell; SCI: spinal cord injury.

corresponded to the injury area (Fig. 6A). As shown in Fig. 6A, the red arrows represent the injured site, and T1WI showed a clear anatomical morphology, but it did not reveal conspicuous variations of the spinal cord after SCI or transplantation. MRI-T2WI images clearly exhibited the repair process after SCI (Fig. 6B). In T2W images, the hyperintense region indicated the injury area, and the image showed that there was a decreased signal intensity surrounding the hyperintense region.

### DTT Images and FA Values

DTT assay was performed to visualize the repair process of spinal cord tracts. The nerve fibers in the spinal cord white matter are clearly presented in Fig. 7A, and the red circles represent the injured site. We could clearly observe the breakage, distortion, depression, and irregularity of nerve fibers. Compared with those in the SCI group, the nerve fibers in the OECs-sh-miR-199a-5p and

OECs-null groups were visually more regular at 3 and 6 wk (Fig. 7A). The FA value was used as a parameter to quantitatively analyze the repair effect of miR-199a-5p suppression in OECs. The FA value directly reflected the degree of spatial displacement of water molecules, and indirectly reflected the axonal integrity. Higher FA values indicated stronger anisotropy and more complete nerve fibers. In injured segments, the FA value decreased sharply after injury and gradually increased with time (Fig. 7B). Compared to those in the SCI group, the FA values in the OECs-sh-miR-199a-5p and OECs-null groups were significantly higher from 1 to 6 wk post transplantation ( $P < 0.05$ ); moreover, the FA values in the OECs-sh-miR-199a-5p group were significantly higher than those in the OECs-null group from 2 to 6 wk ( $P < 0.05$ ) after transplantation (Fig. 7B). According to the slice thickness for the DTI scan, we performed analyses of the different spinal cord segments (+ represented the rostral end, – represented the caudal end) at

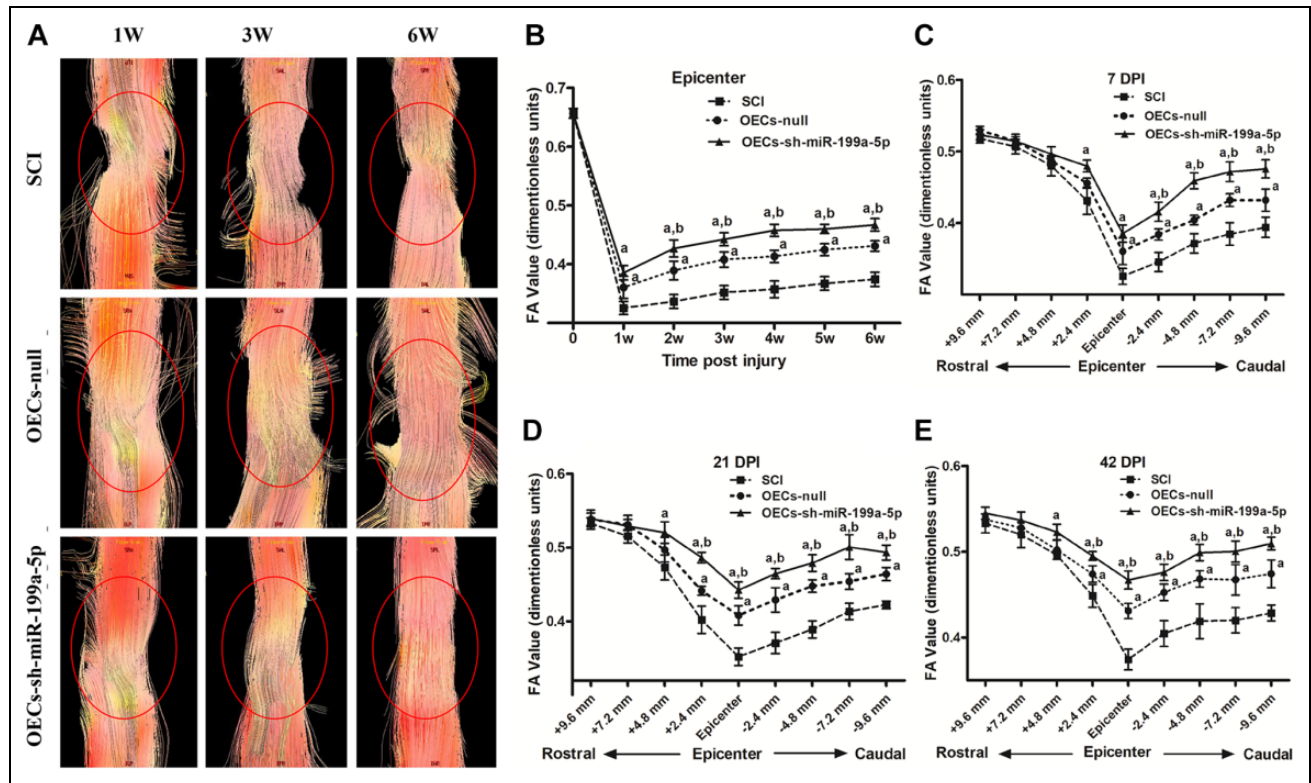


**Fig. 7.** DTT images and quantitative analysis of the diffusion tensor imaging–derived FA values. (A) DTT of the spinal cord in each group. Red circles represent the injured site. (B) The FA values in the injured epicenter in each group. (C) The FA values of the rostral and caudal spinal cord adjacent to the lesioned epicenter at 7 DPI. (D) The FA values of the rostral and caudal spinal cord adjacent to the lesioned epicenter at 21 DPI. (E) The FA values of the rostral and caudal spinal cord adjacent to the lesioned epicenter at 42 DPI. Data from rats ( $n = 6$ ) for each group at each time point or at different spinal segments are represented as the mean  $\pm$  SD. <sup>a</sup> $P < 0.05$  vs SCI group; <sup>b</sup> $P < 0.05$  vs OECs-null group.

DTT: diffusion tensor tractography; DPI: days post injury; FA: fractional anisotropy; OEC: olfactory ensheathing cell; SCI: spinal cord injury.

2.4, 4.8, 7.2, and 9.6 mm away from the epicenter at 7, 21, and 42 DPI. We found that from the rostral end to the epicenter, the FA value gradually decreased and was the lowest in the injury epicenter. Conversely, the FA value gradually increased from the injury epicenter to the caudal end. Furthermore, the FA value in the caudal end was invariably lower than that in the rostral end with the same distance away from the center of damage. The FA value in the OECs-sh-miR-199a-5p group was significantly higher than that in the SCI group at +2.4 mm, epicenter, -2.4 mm, -4.8 mm, -7.2 mm, and -9.6 mm ( $P < 0.05$ ) and was significantly higher than that in the OECs-null group at -2.4 mm, -4.8 mm, and -7.2 mm at 7 DPI ( $P < 0.05$ ) (Fig. 7C). However, there was no significant difference between the three groups at +4.8, +7.2, and +9.6 mm at 7 DPI (Fig. 7C). At 21 and 42 DPI, the FA values showed a consistent trend, and the FA values in the OECs-sh-miR-199a-5p group were significantly higher than those in the OECs-null group and SCI group at +2.4 mm, epicenter, -2.4, -4.8, -7.2, and -9.6 mm ( $P < 0.05$ ), but not at +4.8, +7.2, or +9.6 mm (Fig. 7D, E).

### Histological Changes

H&E staining revealed histological changes at the injury epicenter at 100 $\times$  magnification (Fig. 8). At 1 wk post injury, disorganization of the spinal cord and infiltration of inflammatory cells were clearly visible in the three groups, and there were no apparent differences in the histological changes among the three groups. However, at 3 and 6 wk post OEC transplantation, compared to those in the OEC-null group and SCI group, the cavity, scar formation, and injury area in the OECs-sh-miR-199a-5p group seemed to be smaller.

### NF200 IHC

The expression of NF200 in the injured spinal cord was determined by IHC. The results indicated that the NF200-positive area in the gray matter increased significantly at 3 and 6 wk post injury in all three groups and compared to the SCI group, OECs-sh-miR-199a-5p and OECs-null transplantation facilitated NF200-positive axonal regeneration in the circumambient regions of the injury site (Fig. 9A). The NF200-positive area in the gray matter was analyzed using Image J software.



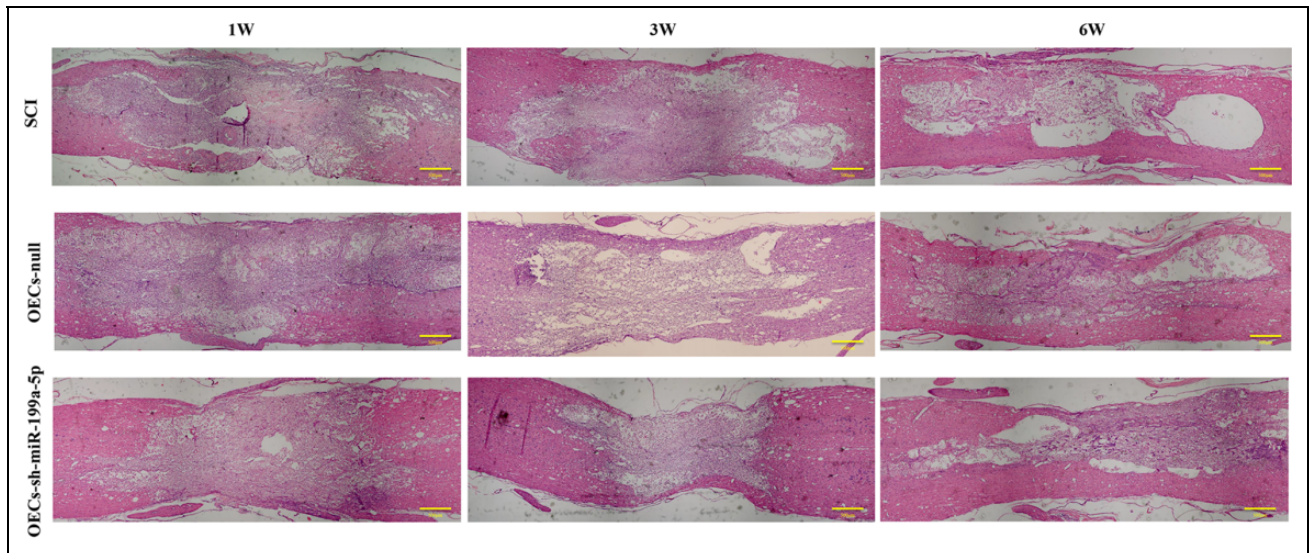


**Fig. 8.** Hematoxylin and eosin staining of the spinal cord after injury or modified OEC transplantation. All cell nuclei were stained dark purple, and the cytoplasm was stained pink. The scale bar is 500  $\mu\text{m}$ . OEC: olfactory ensheathing cell; SCI: spinal cord injury.

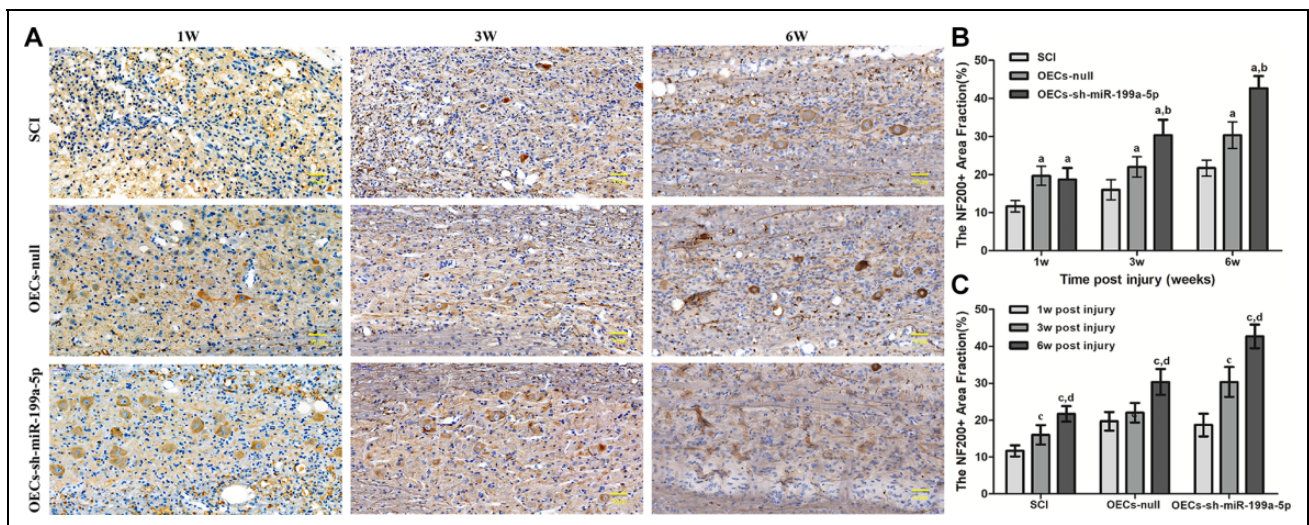


**Fig. 9.** Immunohistochemical staining of NF200 in the region around the injury site. (A) Representative images of NF200 staining. (B) The NF200-positive area fraction of the gray matter at each time point. (C) The NF200-positive area fraction of the gray matter in consecutive time points in each group. NF200-positive axons or neurons were stained brown, and all cell nuclei were stained blue. The scale bar is 50  $\mu\text{m}$ . The NF200-positive area fractions in the gray matter around the lesioned site of the sections from three rats are expressed as the mean  $\pm$  standard deviation. <sup>a</sup> $P < 0.05$  vs SCI group; <sup>b</sup> $P < 0.05$  vs OECs-null group; <sup>c</sup> $P < 0.05$  vs 1 wk post injury; <sup>d</sup> $P < 0.05$  vs 3 wk post injury. NF200: neurofilament-200; OEC: olfactory ensheathing cell; SCI: spinal cord injury.

Statistical results indicated that there were more NF200-positive structures in the OECs-sh-miR-199a-5p and OECs-null groups than in the SCI group at all time points post transplantation ( $P < 0.05$ ). Moreover, the NF200-positive area fraction in the OECs-sh-miR-199a-5p group was significantly higher than that in the OECs-null group at 3 and 6 wk ( $P < 0.05$ ) (Fig. 9B). In addition, the images demonstrated that the NF200-positive area increased gradually with time in the

three groups, and there was an obvious increase between 3 and 6 wk post transplantation (Fig. 9C).

### *Slit1, Robo2, and srGAP2 Are Direct Targets of miR-199a-5p*

To explore the possible mechanism by which miR-199a-5p inhibition induced functional recovery in SCI rats, miR-

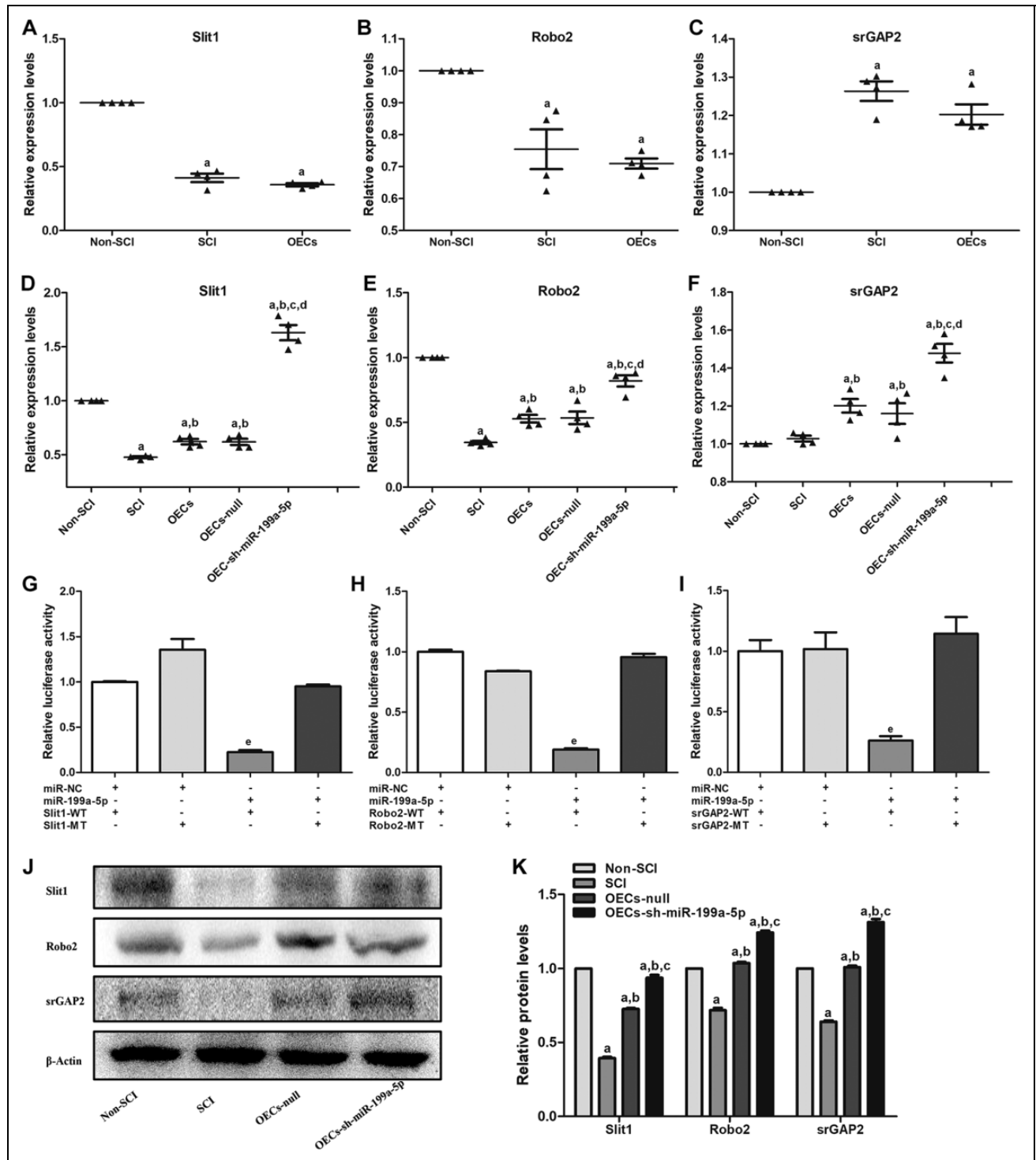


**Fig. 10.** Slit1, Robo2, and srGAP2 are direct targets of miR-199a-5p. Relative mRNA expression of Slit1 (A), Robo2 (B), and srGAP2 (C) in spinal cord with non-SCI, SCI, and OEC transplantation for 1 wk from the microarray data (GSE46988). Relative mRNA expression of Slit1 (D), Robo2 (E), and srGAP2 (F) in spinal cord with non-SCI, SCI, and OECs or modified OEC transplantation for 1 wk were measured by qRT-PCR. (G) Relative luciferase activity after 24 h of co-transfection of Slit1-WT or Slit1-MT and miR-199a-5p mimics or miR negative control (miR-NC) in HEK293 T cells. (H) Relative luciferase activity after 24 h of co-transfection of Robo2-WT or Robo2-MT and miR-199a-5p mimics or miR-NC in HEK293 T cells. (I) Relative luciferase activity after 24 h of co-transfection of srGAP2-WT or srGAP2-MT and miR-199a-5p mimics or miR-NC in HEK293 T cells. (J) The protein levels of Slit1, Robo2, and srGAP2 were measured by western blot in the non-SCI, SCI, OECs-null, and OECs-sh-199a-5p groups. (K) The relative protein levels of Slit1, Robo2, and srGAP2 in each group were analyzed by ImageJ software. All results of target gene mRNA levels are expressed as the mean  $\pm$  SEM from four independent experiments ( $n = 4$ ).  
(to be Continued.)

199a-5p target genes were identified using the computer-aided miRNA target prediction program TargetScan. Putative miR-199a-5p target genes that might play an important role in axon regeneration and neuronal axon guidance included Slit1, Robo2, and srGAP2. We first analyzed the mRNA expression levels of the three target genes in a microarray dataset (GSE46988). The results showed that the mRNA levels of Slit1 and Robo2 in the SCI group were significantly decreased compared with those in the non-SCI group ( $P < 0.05$ ), but not for srGAP2, which showed a significant increase in the SCI group compared with the non-SCI group, while the levels of these target genes in the OECs group did not increase after OEC transplantation (Fig. 10A–C). After SCI or non-SCI and OECs or modified OECs transplantation for 1 wk, we validated the expression levels of Slit1, Robo2, and srGAP2 in vivo by qRT-PCR (Fig. 10D–F). The results showed that the mRNA levels of Slit1 and Robo2 in the SCI group were significantly lower than those in the non-SCI group ( $P < 0.05$ ) but not for srGAP2. The expression levels of Slit1, Robo2, and srGAP2 in the OECs and OECs-null groups were significantly higher compared with those in the SCI group. There was no significant difference between the OECs and OECs-null groups, which indicated that OECs-null did not change OEC-related functions or characteristics. More importantly, the levels of the three target genes in the OECs-sh-miR-199a-5p group were significantly increased compared with those in the OECs-null, OECs, and SCI groups, particularly for Slit1 and srGAP2, which were significantly higher than those in the non-SCI group ( $P < 0.05$ ) (Fig. 10D, F).

We further used the dual-luciferase reporter assay to determine the relationship between miR-199a-5p and Slit1, Robo2, and srGAP2. Results showed that co-transfection of miR-199a-5p mimics and Slit1-WT, Robo2-WT, or srGAP2-WT induced 77.51%, 81.02%, and 73.85% reduction in luciferase activity compared to co-transfection of miR-NC and Slit1-WT, Robo2-WT, or srGAP2-WT, respectively (Fig. 10G–I). The luciferase activity in cells co-transfected with miR-199a-5p mimics and Slit1-WT was significantly decreased compared with that in other transfection groups ( $P < 0.05$ ), and co-transfection of miR-NC and Slit1-WT or co-transfection of mimics and Slit1-MT did not change the luciferase activity ( $P > 0.05$ ) (Fig. 10G). The results with Robo2 and srGAP2 were similar to those with Slit1 (Fig. 10H, I), and co-transfection of miR-199a-5p mimics and Robo2-WT or srGAP2-WT significantly decreased the luciferase activity ( $P < 0.05$ ). Then, we used western blotting to determine whether miR-199a-5p knockdown increased

Slit1, Robo2, and srGAP2 at the protein level. As shown in Fig. 10J, knockdown of miR-199a-5p increased the protein levels of Slit1, Robo2, and srGAP2, and the protein levels in the OECs-sh-miR-199a-5p and OECs-null groups were significantly higher than those of the SCI group ( $P < 0.05$ ) (Fig. 10K). Furthermore, the expression levels in OECs-sh-miR-199a-5p group were higher than those of the OECs-null group ( $P < 0.05$ ) (Fig. 10K). Taken together, our data demonstrated that miR-199a-5p directly targeted Slit1, Robo2, and srGAP2, and knockdown of miR-199a-5p increased their protein levels.

## Discussion

SCI causes substantial miRNA changes, and then miRNAs regulate the protein expression of their target genes at the posttranslational level, leading to cascading physiopathological events, including inflammatory and immune activation, excitotoxicity, oxidative stress, and neuronal activity imbalances<sup>7,8</sup>. At the same time, endogenous repairs and wound-healing processes are also activated quickly, synchronically, and sequentially after injury in order to minimize secondary injury and to rebuild a favorable environment for axon regeneration. All physiopathological events must be accurately regulated; otherwise, they can result in undesirable effects on the lesioned spinal cord, such as cyst formation, tissue fibrosis, and deterioration due to inflammation<sup>31,32</sup>. Strategies that aim to induce the mitigation of these undesirable events are expected to induce neuroprotection and axonal regeneration. OEC transplantation is based on this principle, which can partially inverse the unbalanced physiopathological events, reestablish a favorable microenvironment for neural regeneration, and exert neuroprotection<sup>17,19</sup>. In this process, the repair mechanisms of OECs are not well understood. Although Torres et al.<sup>29</sup> found that OEC transplantation causes the overexpression of genes involved in tissue repair during the acute phase of injury, the authors focused on gene expression rather than miRNA-mediated gene regulation triggered by OEC transplantation.

In this study, we measured miR-199a-5p levels in rat spinal cords with and without SCI, and we found that the SCI significantly increased the miR-199a levels. Several studies have determined the miR-199a expression patterns and functions in neurons and SCI. Xu et al. reported that inhibition of miRNA-199a upregulated Sirt1 expression and induced further neuroprotection in the brain ischemic tolerance of rats<sup>33</sup>. Liu et al. illustrated that SCI significantly increased miR-199a-3p expression, while hindlimb

**Fig. 10.** (Continued). All luciferase activity values are presented as the mean  $\pm$  SEM after normalization to Renilla luciferase activity, and the results were obtained from three independent experiments. The relative protein levels are shown as the mean  $\pm$  SD from three independent experiments. <sup>a</sup> $P < 0.05$  vs non-SCI group; <sup>b</sup> $P < 0.05$  vs SCI group; <sup>c</sup> $P < 0.05$  vs OECs-null group; <sup>d</sup> $P < 0.05$  vs OECs group; <sup>e</sup> $P < 0.05$  vs co-transfection of miR-NC and target-WT version.

miR: microRNA; OEC: olfactory ensheathing cell; SCI: spinal cord injury; SEM: standard error of the mean; WT: wild type.

exercises significantly decreased miR-199a-3p levels, which further promoted activity-dependent plasticity in the injured spinal cord through the mammalian-target-of-rapamycin signaling pathway<sup>15</sup>. Wang et al. demonstrated that *in vivo* inhibition of miR-199a-5p protected against neuronal damage, in accordance with the upregulation of SIRT1 and subsequent deacetylation of p53 in epilepsy model rats<sup>34</sup>. Lv et al. reported that miR-199a can be sequestered by lncRNA-Map2k4, which subsequently promotes FGF1 expression and mouse spinal cord neuron growth<sup>35</sup>. Bao et al. revealed that miR-199a-5p might protect the spinal cord against I/R-induced injury by negatively regulating ECE1 in rats<sup>36</sup>. These findings indicated that miR-199a plays different roles in various disease models. In our study, SCI significantly increased the miR-199a expression, which was consistent with Liu et al. After functional, imageological, and histological evaluations of SCI rats, we confirmed for the first time that the sh-miR-199a-5p-modified OECs showed a better therapeutic effect compared with unmodified OECs for treating SCI rats.

The survival of the grafted OECs in the lesioned spinal cord is the prerequisite for their functions. Therefore, we used GFP-lentiviral vectors to label OECs to observe their survival after transplantation. It was found that despite the cells in injury center being dead, a large number of OECs still survived around the lesions at 1 wk after transplantation. Studies, with the OECs survival rate ranging from 0.3% to 3%, have shown a significant functional recovery<sup>37–39</sup>. In addition, it has been reported that the repair effects of OECs do not depend on the permanent presence of OECs at the site of the injury<sup>40</sup>. In this study, although we cannot measure the proportion of survived OECs at 1 wk after transplantation, our results indicated that OEC transplantation promoted the functional recovery in SCI rats; moreover, modified OECs showed a better neural repair effect. A recent review pointed out that OECs can survive within 1 wk to 1 yr after transplantation<sup>41</sup>. Furthermore, we paid more attention to the gene regulation effects of OECs in SCI rats at 1 wk after transplantation in this study; therefore, we did not explore the survival of OECs after 1 wk.

We silenced miR-199a-5p in OECs by transfecting with sh-miR-199a-5p-lentiviral vectors. In modified cells, the miR-199a-5p expression was significantly inhibited compared to OECs-null, and the efficiency of gene knockdown reached 96.54%, indicating that our transfection experiments were reliable and credible. After transplantation of modified OECs, the miR-199a-5p levels in the whole spinal cord were also significantly inhibited. We speculated that this inhibition may be attributed to the presence of miR-199a-5p-silenced OECs. In addition, the cell-to-cell communication between sh-miR-199a-5p-silenced OECs and spinal neurons or glial cells in injured spinal cord may also affect gene expression in spinal tissue cells, and eventually reduced miR-199a-5p level, which needs further research to explore.

Conventional MRI is one of the vital methodologies in experimental or clinical evaluation of SCI and is regarded as

the gold standard imaging modality<sup>42</sup>. However, it cannot clearly show the severity of the damage and the regeneration process of nerve fibers after injury and only provides an anatomical shape for qualitative assessment. In addition, it has not been shown to consistently relate to the clinical results after SCI. DTI technology can sensitively reflect the subtle pathological and physiological changes of nerve fibers in the injured spinal cord, and it is an accurate, noninvasive imaging method based on the diffusion of water molecules in tissues and provides quantitative information about tissue microstructure, such as axons. It has been demonstrated to be a more sensitive imaging modality for SCI than standard MRI and is widely applied in the diagnosis, treatments, and prognosis of SCI. FA and apparent diffusion coefficient (ADC) values are frequently used quantitative DTI parameters for assessing SCI. FA reflects the diffusion anisotropy of water molecules, and ADC reflects the diffusion magnitude of water molecules. Studies have demonstrated that FA has a better ability than ADC in detecting differences in SCI<sup>42–46</sup>. Therefore, we chose DTI-derived FA instead of the ADC value as the quantitative parameter to evaluate the therapeutic effects of OECs. Based on the diffusion anisotropy of water molecules, FA indirectly reflects the integrity of white matter fibers, including axonal structures. FA values vary between 0 (isotropic diffusion) and 1 (infinite anisotropy), and reduced FA is indicative of degeneration, breakage, or loss of axons.

In the present study, we examined the sequential FA values at the injured epicenter as well as the values at +9.6, +7.2, +4.8, +2.4, -2.4, -4.8, -7.2, and -9.6 mm away from the epicenter (+ represented the rostral, - represented the caudal end) according to the layer thickness (2.4 mm) of the DTI scan. Our results showed that the FA value in the injured site decreased sharply after injury and gradually increased with time. Increased FA values indicated neural restoration consistent with the locomotor rating scale in the respective group. As expected, both OEC and modified OEC transplantation could induce neurorestoration, and modified OECs showed better repair, consistent with higher extremity motor scores and higher FA values. Fig. 7C–E showed that the FA value was the lowest at the epicenter; the farther away from the epicenter, the higher the FA value. This may be explained by pathophysiological changes after SCI, which reveals that, after SCI, the injury site is damaged most severely, accompanied by interruption and disintegration of axons; when secondary injury occurs, axonal disintegration extends from the epicenter toward the rostral and caudal ends but to a lesser degree with increasing distance<sup>47</sup>. Herein, we discovered an FA variation trend consistent with previous results<sup>48,49</sup>. Interestingly, we found that the FA value in the caudal end was invariably lower than that in the rostral end with the same distance away from the damage center at 7, 21, and 42 DPI. This finding was in accordance with a previous study. Since white matter is inherently more anisotropic than gray matter, this discrepancy is likely due to



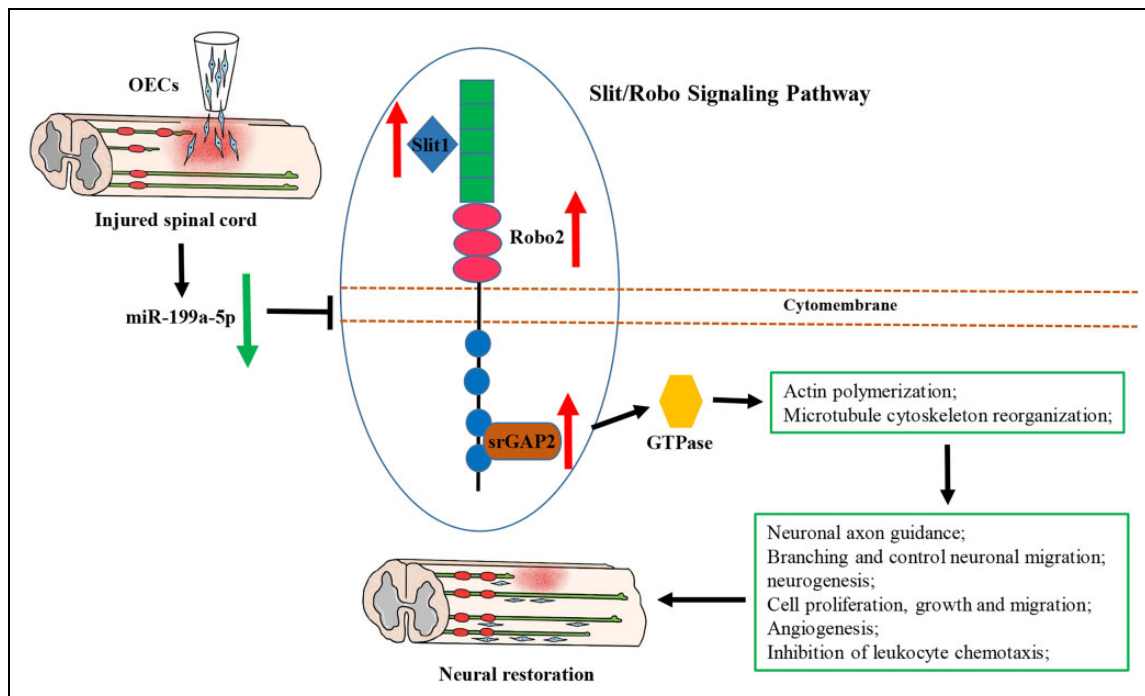


**Fig. 11.** miR-199a-5p downregulation mediates the therapeutic mechanisms of OECs. OEC transplantation downregulated the miR-199a-5p level in injured spinal cord, and then resulted in a significant increase of the protein levels of Slit1, Robo2, and srGAP2. After Slit1 bound to its receptor Robo2, the intracellular region of Robo2 recruited the srGAP2 protein. The protein complex consisting of Robo2 and srGAP2 further activated GTPase, and the latter changed the cytopolarity and cell motility by regulating actin polymerization and microtubule cytoskeletal reorganization. These reactions promoted nerve repair by neuronal axon guidance, controlling neuronal growth and proliferation, neurogenesis, angiogenesis, inhibition of leukocyte chemotaxis, and so on. miR: microRNA; OECs: olfactory ensheathing cells.

the lower ratio of white-to-gray matter in farther caudal segments<sup>48</sup>.

In this study, we first found that Slit1, Robo2, and its downstream molecule srGAP2 have base-pair complementary binding sites with miR-199a-5p, and these axon guidance molecules were involved in the Slit/Robo signaling pathway. Then, the qRT-PCR results showed that the levels of the three target genes in the OECs-sh-miR-199a-5p group significantly increased compared with those in the other groups except for the non-SCI group. In addition, the luciferase activity in cells co-transfected with miR-199a-5p mimics and Slit-WT, Robo2-WT, or srGAP2-WT was significantly decreased compared with that in other transfection groups. Finally, knockdown of miR-199a-5p not only normalized Slit1 protein but increased both Robo2 and srGAP2 above normal spinal cord levels. Taken together, our data indicated that miR-199a-5p directly targeted Slit1, Robo2, and srGAP2 and inhibition of miR-199a-5p increased their protein levels in spinal cord.

Slit1 is a highly conserved secreted glycoprotein that can regulate many physiological processes, such as neuronal axon guidance, cell proliferation, stem cell growth, cell migration, and vascularization<sup>49</sup>. Robo2, the receptors of Slit1, is a transmembrane receptor protein, which mediates downstream signaling cascades by recruiting different

adaptors or proteins<sup>50</sup>. The intracellular region of Robo2 has no autocatalytic or intrinsic enzymatic activity, and when Slit1 binds to the receptor Robo2, the protein complex must depend on downstream regulatory molecules to exert function<sup>50,51</sup>. SrGAP2, the downstream Slit/Robo GTPase activating proteins, is a regulatory molecule associated with actin polymerization and microtubule cytoskeleton reorganization<sup>51</sup>. Slit/Robo signaling is first reported in the nervous system<sup>50</sup>, and studies have substantiated that Slit/Robo signaling has functioned as an extracellular signpost to guide neuronal axon pathfinding and branching and to control neuronal migration<sup>51</sup>, whereafter the function of Slit/Robo signaling has been found to extend far beyond axon guidance and neurocyte development to angiogenesis and inhibition of leukocyte chemotaxis<sup>52-54</sup>. In our study, the protein levels of Slit1, Robo2, and srGAP2 were increased in OECs or modified OECs transplantation group. We believed that the normalization of Slit1 and supranormalization of Robo2 and srGAP2, which were induced by miR-199a-5p knockdown, contributed to the beneficial effects of OEC transplants.

Based on our findings, we speculated that sh-miR-199a-5p may mediate the neural repair effects of OECs in SCI rats through the Slit/Robo signaling pathway. The mechanism could be summarized as follows: OEC transplantation reduced miR-199a-5p expression in the spinal cord tissue,

and then alleviated the silencing effects of miR-199a-5p on Slit1, Robo2, and srGAP2 mRNAs in posttranscriptional level, leading to an increase of target proteins. After Slit1 bound to its receptor Robo2, the intracellular region of Robo2 recruited the srGAP2 protein. The protein complex consisting of Robo2 and srGAP2 further activated GTPase, and the latter changed the cytopolarity and cell motility by regulating actin polymerization and microtubule cytoskeletal reorganization. These reactions promoted nerve repair by neuronal axon guidance, controlling neuronal growth and proliferation, neurogenesis, angiogenesis, inhibition of leukocyte chemotaxis, and so on. The schematic is shown in Fig. 11.

## Conclusion

Our results demonstrated that transplantation of sh-miR-199a-5p-modified OECs promotes functional recovery in SCI rats, suggesting that miR-199a-5p knockdown was more beneficial to the therapeutic effects of OEC transplants, which was probably due to the increase of Slit, Robo2, and srGAP2 proteins. These findings provided new insights into miRNAs-mediated therapeutic mechanisms of OECs, which helps us to develop therapeutic strategies based on miRNAs and optimize cell therapy for SCI.

## Acknowledgments

The authors would like to express their appreciation to Mengchao Gu, Siqi Xu, Yan Liu, and Yuqian Lv for technical help and encouragement.

## Author Contributions

Conceptualization: Su'e Chang and Zhengchao Gao; investigation: Yingjie Zhao and Zikuan Leng; methodology: Zhengchao Gao, Xiaoqian Zhou, Hui Song, Rui Wang, Zhongyang Gao, Yiqun Wang, and Jiantao Liu; resources: Binbin Niu; writing of original draft: Zhengchao Gao and Su'e Chang; manuscript review and editing: Haopeng Li and Pengrong Ouyang; supervision: Xijing He and Su'e Chang; funders: Xijing He and Su'e Chang; co-corresponding authors: Xijing He and Su'e Chang.

## Ethical Approval

This research was approved by the Animal Experiment Committee of Xi'an Jiaotong University.

## Statement of Human and Animal Rights

All of the experimental procedures of this study were conducted in accordance with the protocols approved by Xi'an Jiaotong University Institutional Animal Care and Use Committee.

## Statement of Informed Consent

There were no human subjects in this research, and informed consent was not applicable.


## Declaration of Conflicting Interests


The author(s) declared no potential conflicts of interest with respect to the research, authorship, and/or publication of this article.

## Funding

The author(s) disclosed receipt of the following financial support for the research, authorship, and/or publication of this article: This research was financially supported by the National Natural Science Foundation of China (No. 81571209 and No. 81601081) and The Fundamental Research Funds for the Central Universities (No. xjj2017015).

## ORCID iDs

Zhengchao Gao  <https://orcid.org/0000-0001-8328-9775>

Yingjie Zhao  <https://orcid.org/0000-0002-1873-7807>

## References

- Jazayeri SB, Beygi S, Shokraneh F, Hagen EM, Rahimi Movaghar V. Incidence of traumatic spinal cord injury worldwide: a systematic review. *Eur Spine J.* 2015;24(5):905–918.
- Vierck C. Mechanisms of below-level pain following spinal cord injury (SCI) [published online ahead of print Sep 5, 2019]. *J Pain.* 2019.
- Jorge A, Taylor T, Agarwal N, Hamilton DK. Current agents and related therapeutic targets for inflammation after acute traumatic spinal cord injury. *World Neurosurg.* 2019;132:138–147.
- Martirosyan NL, Carotenuto A, Patel AA, Kalani MY, Yagmurulu K, Lemole GM Jr, Preul MC, Theodore N. The role of microRNA Markers in the diagnosis, treatment, and outcome prediction of spinal cord injury. *Front Surg.* 2016;3:56.
- Shi Z, Zhou H, Lu L, Li X, Fu Z, Liu J, Kang Y, Wei Z, Pan B, Liu L, Kong X, et al. The roles of microRNAs in spinal cord injury. *Int J Neurosci.* 2017;127(12):1104–1115.
- Ning B, Gao L, Liu RH, Liu Y, Zhang NS, Chen ZY. microRNAs in spinal cord injury: potential roles and therapeutic implications. *Int J Biol Sci.* 2014;10(9):997–1006.
- Nieto Diaz M, Esteban FJ, Reigada D, Muñoz Galdeano T, Yunta M, Caballero López M, Navarro Ruiz R, Del Águila A, Maza RM. MicroRNA dysregulation in spinal cord injury: causes, consequences and therapeutics. *Front Cell Neurosci.* 2014;8:53.
- Li F, Zhou M. MicroRNAs in contusion spinal cord injury: pathophysiology and clinical utility. *Acta Neurol Belg.* 2019;119(1):21–27.
- Xu G, Ao R, Zhi Z, Jia J, Yu B. miR-21 and miR-19b delivered by hMSC-derived EVs regulate the apoptosis and differentiation of neurons in patients with spinal cord injury. *J Cell Physiol.* 2019;234(7):10205–10217.
- Jee MK, Jung JS, Im YB, Jung SJ, Kang SK. Silencing of miR20a is crucial for Ngn1-mediated neuroprotection in injured spinal cord. *Hum Gene Ther.* 2012;23(5):508–520.
- Jiao G, Pan B, Zhou Z, Zhou L, Li Z, Zhang Z. MicroRNA-21 regulates cell proliferation and apoptosis in H<sub>2</sub>O<sub>2</sub>-stimulated rat spinal cord neurons. *Mol Med Rep.* 2015;12(5):7011–7016.
- Iyer A, Zurolo E, Prabowo A, Fluiter K, Spliet WG, van Rijen PC, Gorter JA, Aronica E. MicroRNA-146a: a key regulator of astrocyte-mediated inflammatory response. *PLoS One.* 2012;7(9):e44789.

13. Hutchison ER, Kawamoto EM, Taub DD, Lal A, Abdelmohsen K, Zhang Y, Wood WH, Lehrmann E, Camandola S, Becker KG, Gorospe M, et al. Evidence for miR-181 involvement in neuroinflammatory responses of astrocytes. *Glia*. 2013;61(7):1018–1028.
14. Hu J, Zeng L, Huang J, Wang G, Lu H. miR-126 promotes angiogenesis and attenuates inflammation after contusion spinal cord injury in rats. *Brain Res*. 2015;1608:191–202.
15. Liu G, Detloff MR, Miller KN, Santi L, Houle JD. Exercise modulates microRNAs that affect the PTEN/mTOR pathway in rats after spinal cord injury. *Exp Neurol*. 2012;233(1):447–456.
16. Ujigo S, Kamei N, Hadoush H, Fujioka Y, Miyaki S, Nakasa T, Tanaka N, Nakanishi K, Eguchi A, Sunagawa T, Ochi M. Administration of microRNA-210 promotes spinal cord regeneration in mice. *Spine (Phila Pa 1976)*. 2014;39(14):1099–1107.
17. Roet KC, Verhaagen J. Understanding the neural repair-promoting properties of olfactory ensheathing cells. *Exp Neurol*. 2014;261:594–609.
18. Nakhjavan Shahraki B, Youseffard M, Rahimi Movaghar V, Baikpour M, Nasirinezhad F, Safari S, Yaseri M, Moghadas Jafari A, Ghelichkhani P, Tafakhori A, Hosseini M. Transplantation of olfactory ensheathing cells on functional recovery and neuropathic pain after spinal cord injury; systematic review and meta-analysis. *Sci Rep*. 2018;8(1):325.
19. Gómez RM, Sánchez MY, Portela Lomba M, Ghotme K, Barreto GE Sierra J, Moreno Flores MT. Cell therapy for spinal cord injury with olfactory ensheathing glia cells (OECs). *Glia*. 2018;66(7):1267–1301.
20. Guérout N, Derambure C, Drouot L, Bon Mardion N, Duclos C, Boyer O, Marie JP. Comparative gene expression profiling of olfactory ensheathing cells from olfactory bulb and olfactory mucosa. *Glia*. 2010;58(13):1570–1580.
21. Liu Y, Teng X, Yang X, Song Q, Lu R, Xiong J, Liu B, Zeng N, Zeng Y, Long J, Cao R, et al. Shotgun proteomics and network analysis between plasma membrane and extracellular matrix proteins from rat olfactory ensheathing cells. *Cell Transplant*. 2010;19(2):133–146.
22. Woodhall E, West AK, Chuah MI. Cultured olfactory ensheathing cells express nerve growth factor, brain-derived neurotrophic factor, glia cell line-derived neurotrophic factor and their receptors. *Brain Res Mol Brain Res*. 2001;88(1-2):203–213.
23. Boruch AV, Connors JJ, Pipitone M, Deadwyler G, Storer PD, Devries GH, Jones KJ. Neurotrophic and migratory properties of an olfactory ensheathing cell line. *Glia*. 2001;33(3):225–229.
24. Lipson AC, Widenfalk J, Lindqvist E, Ebendal T, Olson L. Neurotrophic properties of olfactory ensheathing glia. *Exp Neurol*. 2003;180(2):167–171.
25. Wewetzer K, Grothe C, Claus P. *In vitro* expression and regulation of ciliary neurotrophic factor and its alpha receptor subunit in neonatal rat olfactory ensheathing cells. *Neurosci Lett*. 2001;306(3):165–168.
26. Fairless R, Frame MC, Barnett SC. N-cadherin differentially determines Schwann cell and olfactory ensheathing cell adhesion and migration responses upon contact with astrocytes. *Mol Cell Neurosci*. 2005;28(2):253–263.
27. Witheford M, Westendorf K, Roskams AJ. Olfactory ensheathing cells promote corticospinal axonal outgrowth by a L1 CAM-dependent mechanism. *Glia*. 2013;61(11):1873–1889.
28. Lee WS, Lee WH, Bae YC. Axon Guidance Molecules Guiding Neuroinflammation. *Exp Neurobiol*. 2019;28(3):311–319.
29. Torres Espín A, Hernández J, Navarro X. Gene expression changes in the injured spinal cord following transplantation of mesenchymal stem cells or olfactory ensheathing cells. *PLoS One*. 2013;8(10):e76141.
30. Young W. Spinal cord contusion models. *Prog Brain Res*. 2002;137:231–255.
31. Teller P, White TK. The physiology of wound healing: injury through maturation. *Surg Clin North Am*. 2009;89(3):599–610.
32. Velnar T, Bailey T, Smrkolj V. The wound healing process: an overview of the cellular and molecular mechanisms. *J Int Med Res*. 2009;37(5):1528–1542.
33. Xu WH, Yao XY, Yu HJ, Huang JW, Cui LY. Downregulation of miR-199a may play a role in 3-nitropropionic acid induced ischemic tolerance in rat brain. *Brain Res*. 2012;1429:116–123.
34. Wang D, Li Z, Zhang Y, Wang G, Wei M, Hu Y, Ma S, Jiang Y, Che N, Wang X, Yao J, et al. Targeting of microRNA-199a-5p protects against pilocarpine-induced status epilepticus and seizure damage via SIRT1-p53 cascade. *Epilepsia*. 2016;57(5):706–716.
35. Lv HR. lncRNA-Map2k4 sequesters miR-199a to promote FGF1 expression and spinal cord neuron growth. *Biochem Biophys Res Commun*. 2017;490(3):948–954.
36. Bao N, Fang B, Lv H, Jiang Y, Chen F, Wang Z, Ma H. Upregulation of miR-199a-5p protects spinal cord against ischemia/ reperfusion-induced injury via downregulation of ECE1 in rat. *Cell Mol Neurobiol*. 2018;38(6):1293–1303.
37. Salehi M, Pasbakhsh P, Soleimani M, Abbasi M, Hasanzadeh G, Modaresi MH, Sobhani A. Repair of spinal cord injury by co-transplantation of embryonic stem cell-derived motor neuron and olfactory ensheathing cell. *Iran Biomed J*. 2009;13(3):125–135.
38. Amemori T, Jendelova P, Ruzickova K, Arboleda D, Sykova E. Co-transplantation of olfactory ensheathing glia and mesenchymal stromal cells does not have synergistic effects after spinal cord injury in the rat. *Cytherapy*. 2012;12(2):212–225.
39. Li Y, Yu HL, Chen LF, Duan CX, Zhang JY, Li BC. Survival and number of olfactory ensheathing cells transplanted in contused spinal cord of rats. *Chin J Traumatol*. 2010;13(6):356–361.
40. Li Y, Li D, Raisman G. Functional Repair of Rat Corticospinal Tract Lesions Does Not Require Permanent Survival of an Immunoincompatible Transplant. *Cell Transplant*. 2016;25(2):293–299.
41. Reshamwala R, Shah M, John JS, Ekberg J. Survival and integration of transplanted olfactory ensheathing cells are crucial for spinal cord injury repair: insights from the last 10 years of

- animal model studies. *Cell Transplant.* 2019;28(1\_suppl):132S–159S.
42. Ellingson BM, Salamon N, Holly LT. Imaging techniques in spinal cord injury. *World Neurosurg.* 2014;82(6):1351–1358.
  43. Freund P, Wheeler Kingshott C, Jackson J, Miller D, Thompson A, Ciccarelli O. Recovery after spinal cord relapse in multiple sclerosis is predicted by radial diffusivity. *Mult Scler.* 2010;16(10):193–202.
  44. Mondragon Lozano R, Diaz Ruiz A, Ríos C, Olayo Gonzalez R, Favila R, Salgado Ceballos H, Roldan Valadez E. Feasibility of in vivo quantitative magnetic resonance imaging with diffusion weighted imaging, T2-weighted relaxometry, and diffusion tensor imaging in a clinical 3 tesla magnetic resonance scanner for the acute traumatic spinal cord injury of rats: technical note. *Spine (Phila Pa 1976).* 2013;38(20):E1242–E1249.
  45. Li XH, Li JB, He XJ, Wang F, Huang SL, Bai ZL. Timing of diffusion tensor imaging in the acute spinal cord injury of rats. *Sci Rep.* 2015;5:12639.
  46. Sun W, Tan J, Li Z, Lu S, Li M, Kong C, Hai Y, Gao C, Liu X. Evaluation of hyperbaric oxygen treatment in acute traumatic spinal cord injury in rats using diffusion tensor imaging. *Aging Dis.* 2018;9(3):391–400.
  47. Ju G, Wang J, Wang Y, Zhao X. Spinal cord contusion. *Neural Regen Res.* 2014;9(8):789–794.
  48. Patel SP, Smith TD, VanRooyen JL, Powell D, Cox DH, Sullivan PG, Rabchevsky AG. Serial diffusion tensor imaging in vivo predicts long-term functional recovery and histopathology in rats following different severities of spinal cord injury. *J Neurotrauma.* 2016;33(10):917–928.
  49. Zhao C, Rao JS, Pei XJ, Lei JF, Wang ZJ, Zhao W, Wei RH, Yang ZY, Li XG. Diffusion tensor imaging of spinal cord parenchyma lesion in rat with chronic spinal cord injury. *Magn Reson Imaging.* 2018;47:25–32.
  50. Ballard MS, Hinck L. A roundabout way to cancer. *Adv Cancer Res.* 2012;114:187–235.
  51. Dickson BJ, Gilestro GF. Regulation of commissural axon pathfinding by slit and its Robo receptors. *Annu Rev Cell Dev Biol.* 2006;22:651–675.
  52. Tong M, Jun T, Nie Y, Hao J, Fan D. The Role of the Slit/Robo Signaling Pathway. *J Cancer.* 2019;10(12):2694–2705.
  53. Blockus H, Chédotal A. Slit-Robo signaling. *Development.* 2016;43(17):3037–3044.
  54. Chédotal A. Roles of axon guidance molecules in neuronal wiring in the developing spinal cord. *Nat Rev Neurosci.* 2019;20(7):380–396.